

# Azimuthal correlations of hadrons and fragments in nucleus-nucleus collisions<sup>\*</sup>

LI Hui-Ling(李惠玲)<sup>1)</sup>

Institute of Modern Physics, Shanxi Normal University, Linfen 041004, China

**Abstract:** Two-particle (two-fragment) azimuthal correlation functions are studied by using a simple formula which describes uniformly azimuthal distributions of final-state charged particles and nuclear fragments. This formula is obtained in the framework of a multi-source thermal model (or multi-source ideal gas model). The calculated results are compared and found to be in agreement with the experimental data of charged hadrons and nuclear fragments in nucleus-nucleus collisions at intermediate and high energies.

**Key words:** azimuthal correlations, charged particles, nuclear fragments, nucleus-nucleus collisions, intermediate and high energies

**PACS:** 25.75.Gz, 25.75.Ld, 24.10.Pa      **DOI:** 10.1088/1674-1137/35/12/005

## 1 Introduction

Charged particles and nuclear fragments are the main products in nucleus-nucleus collisions at intermediate and high energies. In such collisions, the particles' (and fragments') azimuthal anisotropy and their correlations can provide information on the properties of an interacting system [1–3]. The primary goal of current high energy nuclear physics research is the creation and study of nuclear matter at high energies and high densities. From intermediate energy to high energy regions, nuclear reaction mechanisms are expected to change due to different energy densities. As quantities measured in experiments, azimuthal distributions and correlations can be obtained in intermediate and high energy nucleus-nucleus collisions.

Generally, the azimuthal distributions can be described by a Fourier decomposition [4, 5]

$$\frac{dN}{d(\phi - \Phi_R)} \propto \left( 1 + \sum_{n=1}^{\infty} 2v_n \cos[n(\phi - \Phi_R)] \right), \quad (1)$$

where  $N$  denotes the particle (fragment) number,  $\phi$  is the azimuthal angle of an emitted particle (fragment) and  $\Phi_R$  is the azimuth of the reaction plane which is defined by the beam direction and the impact param-

eter vector. The coefficient  $v_n$  is the  $n$ th-harmonic coefficient of the Fourier expansion of the azimuthal distribution and given by  $v_n = \langle \cos[n(\phi - \Phi_R)] \rangle$ , where  $\langle \dots \rangle$  denote the statistical averaging over particles (fragments) and events. The second moment of the anisotropy flow  $v_2$  is called the elliptic flow which is observed mainly in semi-central nucleus-nucleus collisions at intermediate and high energies. In such collisions, elliptic flows of different charged particles and nuclear fragments result from hydrodynamic pressure gradients developed in a locally thermalized “almond-shaped” collision (participant) zone [6].

An alternative technique for elliptic flow analysis is the Fourier decomposition of the pairwise distribution in the azimuthal angle difference ( $\Delta\phi = \phi_1 - \phi_2$ ) between pairs of emitted particles (fragments) [7–9]:

$$\frac{dN}{d\Delta\phi} \propto \left[ 1 + \sum_{n=1}^{\infty} 2v_n^2 \cos(n\Delta\phi) \right], \quad (2)$$

where the square of the second Fourier coefficient,  $v_2^2$ , characterizes the magnitude of the elliptic flow in this case. Eq. (2) is in fact the  $\Delta\phi$  distribution. Following an approach commonly exploited in interferometry studies, a two-particle (fragment) azimuthal correlation function can be defined as follows [7–9]:

Received 2 March 2011

<sup>\*</sup> Supported by National Natural Science Foundation of China (10975095, 11075100), the Natural Science Foundation of Shanxi Province (2007011005, 2011011001-2) and the Developing Project of Science and Technology of Shanxi Province (20091016)

1) E-mail: lihuilingxyx@sina.com

©2011 Chinese Physical Society and the Institute of High Energy Physics of the Chinese Academy of Sciences and the Institute of Modern Physics of the Chinese Academy of Sciences and IOP Publishing Ltd

$$C(\Delta\phi) = \frac{N_{\text{cor}}(\Delta\phi)}{N_{\text{uncor}}(\Delta\phi)}, \quad (3)$$

where  $N_{\text{cor}}(\Delta\phi)$  is the observed  $\Delta\phi$  distribution for charged particle (fragment) pairs selected from the same event, and  $N_{\text{uncor}}(\Delta\phi)$  is the  $\Delta\phi$  distribution for particle (fragment) pairs selected from mixed events.

Many models have been introduced to describe particle productions in high energy collisions. For example, the FRITIOF model [10], the VENUS model [11, 12], the Gribov-Glauber model [13], the QGSM model [14], the RQMD model [15–17], the Hydrodynamics model [18, 19], the string percolation model [20], the ART model [21], the ZPC model [22], a running coupling non-linear evolution [23], the HIJING model [24–26], a multiphase transport model (the AMPT model) [27], the color glass condensate (CGC) model [28], the perturbative QCD plus saturation plus hydrodynamics (EKRT) model [29], a combination model of constituent quarks and Landau hydrodynamics [30], a two-stage gluon model or a gluon dominance model [31], the KKT model [32], a consistent quantum mechanical multiple scattering approach (EPOS) [33, 34], a multi-source thermal model (or multi-source ideal gas model) [35–44], etc.

In this work, we shall use the multi-source thermal model [35–44] to describe the two-particle (fragment) correlations in nucleus-nucleus collisions at intermediate and high energies. This model contains anisotropic expansions and movements of the participant region in the transverse momentum-space. A simple formula obtained by this model will describe uniformly the azimuthal correlations in different collisions at different energies.

## 2 The model

Although the multi-source thermal model on transverse momentum and azimuthal distributions can be found in references [35–38], a short description is given in the following to show a whole presentation of this work. In the model, let the beam direction be the  $\overline{oz}$  axis and the reaction plane be the  $\overline{xoz}$  plane. Many emission sources (or thermal sources) of particles (fragments) are assumed to form in participant (spectator) in nucleus-nucleus collisions at intermediate and high energies. Each emission source is treated as an ideal gas source in its rest frame. The interactions among different emission sources affect the emissions of particles (fragments).

As in Maxwell's ideal gas model, the three components  $p'_x$ ,  $p'_y$ , and  $p'_z$  of the particle (fragment) mo-

mentum in the rest frame of the emission source obey Gaussian distribution and have the same standard deviation  $\sigma$ , that is [35–38]

$$f_{p'_{x,y,z}}(p'_{x,y,z}) = \frac{1}{\sqrt{2\pi}\sigma} \exp\left(-\frac{p'^2_{x,y,z}}{2\sigma^2}\right). \quad (4)$$

Considering the interactions among different emission sources, the considered source will have expansion and movement in the momentum space. Due to this expansion and movement, the momentum components  $p_x$ ,  $p_y$ , and  $p_z$  of the particle (fragment) momentum in a final state will depart from the Gaussian distribution.

We need only  $p_x$  and  $p_y$  to consider azimuthal distribution and correlation. The simplest relationships between  $p_{x,y}$  and  $p'_{x,y}$  are linear

$$p_{x,y} = a_{x,y}p'_{x,y} + B_{x,y} = a_{x,y}p'_{x,y} + b_{x,y}\sigma, \quad (5)$$

where  $B_{x,y}$  represent the movements of the sources and  $a_{x,y}$  and  $b_{x,y}$  are the coefficients that describe the effects of the expansion and movement of the source respectively [35–38]. It seems that Eq. (5) is in contradiction with the Lorentz transformation. We point out that one could understand the current formalism because Eq. (5) represents the relationships between “mean” momenta in the cases of laboratory (or center-of-mass) reference frame and source rest frame.

The azimuthal momentum-space anisotropy of particles (fragments) produced in nucleus-nucleus collisions at intermediate and high energies can be described by the momentum components, we have the azimuthal angle

$$\phi = \arctan \frac{p_y}{p_x}. \quad (6)$$

The transverse momentum  $p_T$  is also given by the momentum components, that is

$$p_T = \sqrt{p_x^2 + p_y^2}. \quad (7)$$

According to the knowledge of probability theory and Eq. (5), the distributions of  $p_{x,y}$  can be given by [35–38]

$$f_{p_{x,y}}(p_{x,y}) = \frac{1}{\sqrt{2\pi}\sigma a_{x,y}} \exp\left[-\frac{(p_{x,y} - b_{x,y}\sigma)^2}{2\sigma^2 a_{x,y}^2}\right]. \quad (8)$$

The unit-density functions of  $p_x$  and  $p_y$  are [38]

$$\begin{aligned} f_{p_x, p_y}(p_x, p_y) &= f_{p_x}(p_x) f_{p_y}(p_y) \\ &= \frac{1}{2\pi\sigma^2 a_x a_y} \exp\left[-\frac{(p_x - b_x\sigma)^2}{2\sigma^2 a_x^2} - \frac{(p_y - b_y\sigma)^2}{2\sigma^2 a_y^2}\right]. \end{aligned} \quad (9)$$

Then, we have the unit-density functions of  $p_T$  and  $\phi$

as [38]

$$f_{p_T, \phi}(p_T, \phi) = p_T f_{p_x, p_y}(p_T \cos \phi, p_T \sin \phi) \\ = \frac{p_T}{2\pi\sigma^2 a_x a_y} \exp \left[ -\frac{(p_T \cos \phi - b_x \sigma)^2}{2\sigma^2 a_x^2} - \frac{(p_T \sin \phi - b_y \sigma)^2}{2\sigma^2 a_y^2} \right]. \quad (10)$$

From Eq. (10), we have the  $\phi$  distribution to be

$$f_\phi(\phi) = \int_0^\infty f_{p_T, \phi}(p_T, \phi) dp_T \quad (11)$$

and the  $p_T$  distribution to be

$$f_{p_T}(p_T) = \int_0^{2\pi} f_{p_T, \phi}(p_T, \phi) d\phi. \quad (12)$$

Generally, Eq. (11) can be used to describe the azimuthal distributions of final-state particles and nuclear fragments produced in nucleus-nucleus collisions at intermediate and high energies. According to Eq. (3), the azimuthal correlation is given by

$$C(\Delta\phi) = \int_0^{\Delta\phi} f_\phi(\phi_1) f_\phi(\phi_1 - \Delta\phi) d\phi_1 \\ \Big/ \int_0^{\Delta\phi} f'_\phi(\phi_1) f'_\phi(\phi_1 - \Delta\phi) d\phi_1, \quad (13)$$

where  $f'_\phi$  denotes the azimuthal distribution of particles from mixed events and equals  $f_\phi$  with  $a_{x,y} = 1$  and  $b_{x,y} = 0$ .

It is difficult to give a set of parameters to describe the experimental data by using Eq. (13) due to too many parameters. In calculations, replacing  $\phi$  by  $\Delta\phi$  in Eq. (11), we describe empirically the azimuthal correlations. That is, we have the azimuthal correlation as

$$f_{\Delta\phi}(\Delta\phi) = \int_0^\infty \frac{p_T}{2\pi\sigma^2 a_x a_y} \exp \left[ -\frac{(p_T \cos \Delta\phi - b_x \sigma)^2}{2\sigma^2 a_x^2} - \frac{(p_T \sin \Delta\phi - b_y \sigma)^2}{2\sigma^2 a_y^2} \right] dp_T. \quad (14)$$

In the calculation of  $f_\phi(\phi)$  and  $f_{\Delta\phi}(\Delta\phi)$ , the value of  $\sigma$  does not significantly affect the result. The default values of the four parameters are  $a_{x,y} = 1$  and  $b_{x,y} = 0$ . The physics condition gives  $a_{x,y} \geq 1$ .

### 3 Comparison with experimental data

Figure 1 shows the representative  $\Delta\phi$  correlation functions obtained by the PHENIX collaboration (circles [45]) for charged hadrons detected in the pseudo-rapidity range  $-0.35 < \eta < 0.35$ . The experimental data [45] are presented for different centrality and

$p_T$  ranges in Au-Au collisions at the center-of-mass energy  $\sqrt{s_{NN}} = 130$  GeV. Correspondingly, the calculated curves are given in the figure with different  $a_x$  values as marked in the panels, and the other parameters ( $a_y$  and  $b_{x,y}$ ) are taken to be the default values. In the selection of the parameter values, the method of  $\chi^2$ -testing is used. From the left to right and up to down panels, the obtained values of  $\chi^2$  per degree of freedom ( $\chi^2/\text{dof}$ ) are 0.019, 0.051, 0.051, and 0.100, respectively. One can see that our modelling results are in good agreement with the experimental data of the PHENIX collaboration.

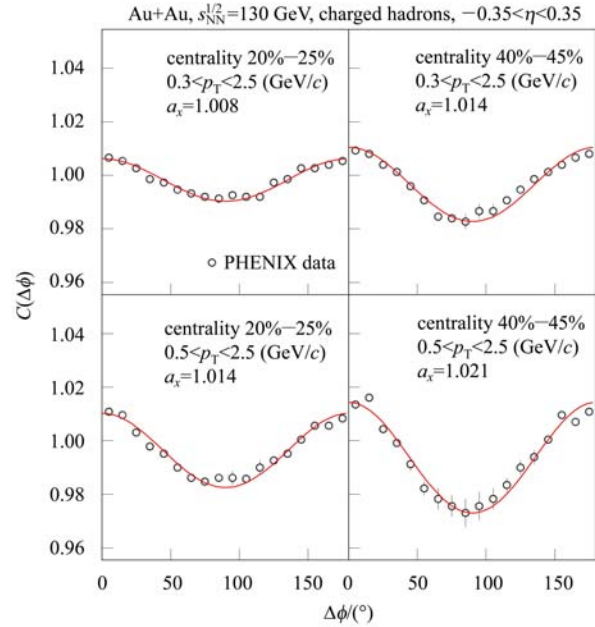


Fig. 1. The azimuthal correlation function for charged hadrons with  $-0.35 < \eta < 0.35$  and different centralities and transverse momenta in Au-Au collisions at  $\sqrt{s_{NN}} = 130$  GeV. The circles represent the experimental data of the PHENIX collaboration [45] and the curves are our calculated results.

The azimuthal correlation function for fragments with rapidity ( $y$ ) greater than  $0.75y_{\text{beam}}$  for Ar-BaI<sub>2</sub> collisions at 1.2 GeV/nucleon in three  $M^*$  intervals and for Ar-KCl collisions at 1.2 GeV/nucleon in a single  $M^*$  interval is presented in Fig. 2, where  $y_{\text{beam}}$  denotes the beam rapidity, and  $M^*$  is defined as a reduced multiplicity counting only fragments over an emission angle range of between  $8^\circ$  and  $85^\circ$ . The circles represent the experimental data of Wang et al [7]. The solid curves are our calculated results with different  $b_x$  values as marked in the panels, and the other parameters are taken to be the default values. The obtained values of  $\chi^2/\text{dof}$  are 0.020, 0.037, 0.024, and

0.041, respectively. To give a comparison, the calculation result with  $a_x = 1.015$ ,  $b_x = 0.068$ ,  $a_y = 1$ , and  $b_y = 0$  for Ar-KCl collisions is drawn in the figure by the dotted curve with  $\chi^2/\text{dof} = 0.029$ . We see that the modelling results with given parameters are in good agreement with the experimental data.

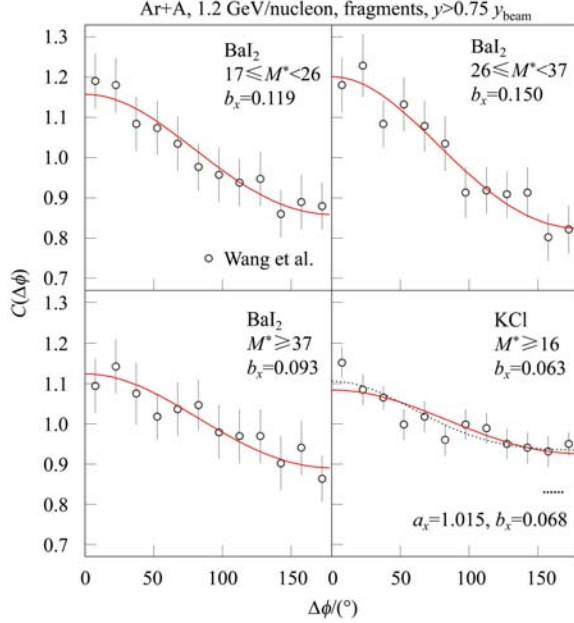


Fig. 2. The azimuthal correlation function for fragments with  $y > 0.75y_{\text{beam}}$  and in different  $M^*$  bins for Ar-BaI<sub>2</sub> and Ar-KCl collisions at 1.2 GeV/nucleon. The circles represent the experimental data of Wang et al [7] and the curves are our calculated results.

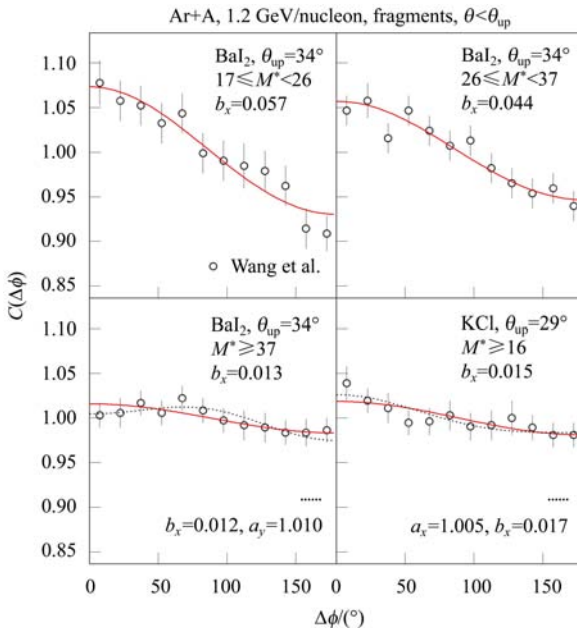


Fig. 3. As in Fig. 2, except that fragments have a maximum emission angle of  $\theta_{\text{up}}$ .

Similar to Fig. 2, the azimuthal correlation function for fragments with emission angle ( $\theta$ ) less than  $\theta_{\text{up}} = 34^\circ$  for Ar-BaI<sub>2</sub> collisions and  $\theta_{\text{up}} = 29^\circ$  for Ar-KCl collisions at 1.2 GeV/nucleon are given in Fig. 3. The obtained values of  $\chi^2/\text{dof}$  are 0.017, 0.014, 0.006, and 0.009, respectively. The calculation result with  $a_x = 1$ ,  $b_x = 0.012$ ,  $a_y = 1.010$ , and  $b_y = 0$  for Ar-BaI<sub>2</sub> collisions in the  $M^* \geq 37$  interval, and that with  $a_x = 1.005$ ,  $b_x = 0.017$ ,  $a_y = 1$ , and  $b_y = 0$  for Ar-KCl collisions are drawn in the figure by the dotted curves with  $\chi^2/\text{dof} = 0.005$  and 0.008 respectively. Once more we see that the modelling results describe well the experimental data [7].

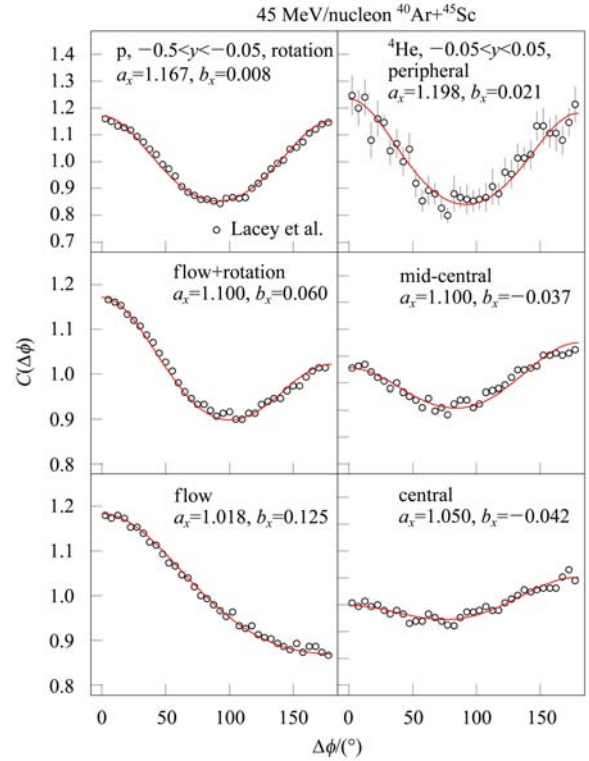


Fig. 4. The left panel: The azimuthal correlation function in simulated  $^{40}\text{Ar} + ^{45}\text{Sc} \rightarrow \text{p} + \text{X}$  at 45 MeV/nucleon for different reaction dynamics. Right panel: The azimuthal correlation function in experimental  $^{40}\text{Ar} + ^{45}\text{Sc} \rightarrow ^4\text{He} + \text{X}$  at 45 MeV/nucleon for different centralities. The circles represent the results of Lacey et al [8] and the curves are our calculated results.

The azimuthal correlation function for  $^{40}\text{Ar} + ^{45}\text{Sc} \rightarrow \text{p} + \text{X}$  and  $^{40}\text{Ar} + ^{45}\text{Sc} \rightarrow ^4\text{He} + \text{X}$  at 45 MeV/nucleon for fragments emitted in different rapidity ranges is displayed in Fig. 4. The circles in the left panel represent the simulated results of Lacey et al. for different reaction dynamics [8], and those

in the right one represent the experimental data of Lacey et al. for different centralities [8]. The curves are our calculated results with different  $a_x$  and  $b_x$  as marked in the panels and the default  $a_y$  ( $= 1$ ) and  $b_y$  ( $= 0$ ). In the calculation, the obtained  $\chi^2/\text{dof}$  are 0.151, 0.036, 0.085, 0.425, 0.069, and 0.257, respectively. One can see that our model describes well the simulated results (left panel) and experimental data (right panel) of Lacey et al [8].

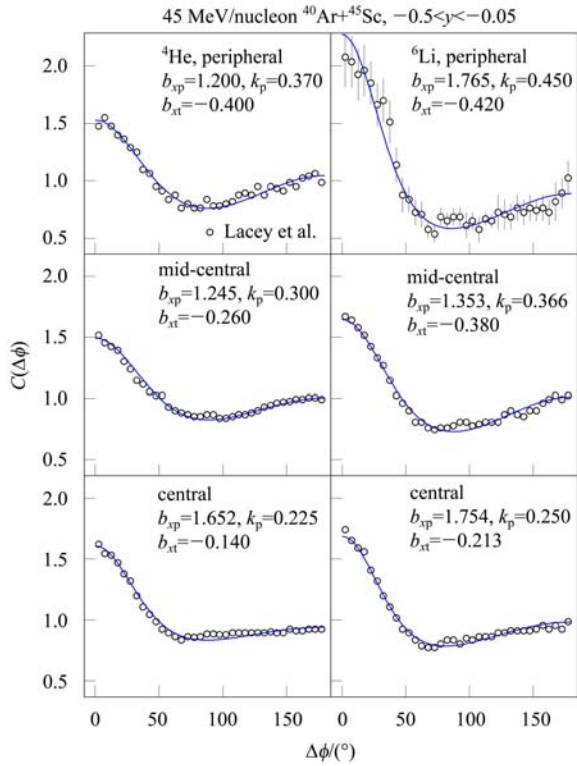


Fig. 5. The azimuthal correlation function in  ${}^{40}\text{Ar} + {}^{45}\text{Sc} \rightarrow {}^4\text{He} + \text{X}$  (left panel) and  ${}^{40}\text{Ar} + {}^{45}\text{Sc} \rightarrow {}^6\text{Li} + \text{X}$  (right panel) at 45 MeV/nucleon for different centralities. The circles represent the experimental data of Lacey et al. [8] and the curves are our calculated results.

Figure 5 shows the azimuthal correlation function for  ${}^{40}\text{Ar} + {}^{45}\text{Sc} \rightarrow {}^4\text{He} + \text{X}$  and  ${}^{40}\text{Ar} + {}^{45}\text{Sc} \rightarrow {}^6\text{Li} + \text{X}$  at 45 MeV/nucleon for fragments emitted in rapidity ranges  $-0.5 < y < -0.05$  and different centralities. The circles represent the experimental data of Lacey et al. [8], and the curves are our calculated results. Differing from Figs. 1–4, we have used a two-component distribution which describes, respectively, the contributions of the projectile and target components. In the figure, except for the default values, the parameters corresponding to the projectile and target components are  $b_{xp}$  and  $b_{xt}$  respectively. The contribution of the projectile component is mainly in the

low  $\Delta\phi$  range, and its fraction is  $k_p$ . The contribution of the target component is mainly in the high  $\Delta\phi$  range, and its fraction is  $1 - k_p$ . In the calculation, the obtained  $\chi^2/\text{dof}$  are 1.773, 0.089, 0.575, 1.419, 0.865, and 0.979, respectively. One can see that our model describes well the experimental data of Lacey et al. [8].

## 4 Conclusion and discussion

To conclude, a multi-source thermal model is used to give a new and simple description of the two-particle (fragment) azimuthal correlation function in nucleus-nucleus collisions at intermediate and high energies. In most cases (Figs. 1–4), a single component distribution describes the experimental data. In another case (Fig. 5), a two-component distribution is used. The calculated results of the multi-source thermal model are in agreement with the considered experimental data. The parameters  $a_{x,y}$  and  $b_{x,y}$  describe the effects of the expansions and movements of the thermal source in the transverse plane respectively.  $a_{x,y} > 1$  means an expansion.  $b_{x,y} > 0$  and  $< 0$  correspond to the source movements along the positive and negative axes respectively. An isotropic emission in the transverse plane presents that  $a_{x,y} = 1$  and  $b_{x,y} = 0$ . The physics condition gives  $a_{x,y} \geq 1$ .

The parameter values for Fig. 1 and for the right panel of Fig. 4 show that the expansion effect of the thermal source decreases with the increase of the centrality. The movement effect in the peripheral collisions is positive, and that in the central collisions is negative. The parameter values for the left panel of Fig. 4 show that the expansion effect in the rotation events is greater than that in the flow events, and the situation of the movement effect is opposite to that. With an increase of fragment multiplicity  $M^*$ , the movement effect for Fig. 2 does not show an obvious change, and that for Fig. 3 decreases obviously. With an increase in centrality, the parameter  $b_{xp}$  for the left panel of Fig. 5 increases obviously, and that for the right panel of Fig. 5 does not show an obvious change. Both  $|b_{xt}|$  and  $k_p$  for Fig. 5 decrease with the increase of the centrality.

The important physical parameters in this model are  $a_{x,y}$  and  $b_{x,y}$ , which describe the effects of the expansions and movements of the thermal source in the transverse plane respectively. Fixing the parameter  $a_y = 1$  in calculations, we obtained the values of  $a_x > 1$  while fitting the experimental data, which physically means an existence of anisotropy in the emission of hadrons in the transverse plane. Also the

values of the parameter  $b_{x,y}$ , describing the movement of the thermal source, were fixed at different values. The simple model used by us for describing the experimental data seems to work and fit the experimental data quite well. In calculations, before getting the values of parameters, we first described the experimental data without fixing the parameters  $a_{x,y}$  and  $b_{x,y}$ . Then, we obtained the values of  $a_x$  not equal to

$a_y$ , this would also prove the existence of anisotropy in experimental data. For example, we fitted the data letting  $a_x$  and  $a_y$  vary, but at fixed values of  $b_{x,y}$  in some intervals of  $b_{x,y}$ , changing  $b_{x,y}$  every time with some equal step  $db_{x,y}$ . After fitting the data many times, we found that the limitation of the physics condition and consideration of relative expansion could give a better result.

## References

- 1 Ackermann K H et al. (STAR collaboration). Phys. Rev. Lett., 2001, **86**: 402
- 2 Adler S S et al. (PHENIX collaboration). Phys. Rev. Lett., 2005, **94**: 232302
- 3 Lacey R A. Nucl. Phys. A, 2006, **774**: 199
- 4 Gutbrod H H et al. Phys. Rev. C, 1990, **42**: 640
- 5 Borghini N, Dinh P M, Ollitrault J Y. Phys. Rev. C, 2001, **64**: 054901
- 6 Afanasiev S et al. (PHENIX collaboration). Phys. Rev. Lett., 2007, **99**: 052301
- 7 WANG S et al. Phys. Rev. C, 1991, **44**: 1091
- 8 Lacey R A et al. Phys. Rev. Lett., 1993, **70**: 1224
- 9 Lacey R et al. (PHENIX collaboration). Nucl. Phys. A, 2002, **698**: 559c
- 10 Gustafson G. Nucl. Phys. A, 1994, **566**: 233c
- 11 Werner K. Phys. Rep., 1993, **232**: 87
- 12 Werner K. Nucl. Phys. A, 1994, **566**: 477c
- 13 Tywoniuk K, Arsene I C, Bravina L, Kaidalov A B, Zabrodin E. arXiv:0705.1596 [hep-ph]
- 14 Bravina L V, Csernai L P, Levai P, Amelin N S, Strottman D. Nucl. Phys. A, 1994, **566**: 461c
- 15 Sorge H, Stöcker H, Greiner W. Nucl. Phys. A, 1989, **498**: 567c
- 16 Sorge H, von Keitz A, Mattiello R, Stocker H, Greiner W. Nucl. Phys. A, 1991, **525**: 95c
- 17 Jahns A, Spieles C, Mattiello R, Amelin N S, Stoecker H, Greiner W, Sorge H. Nucl. Phys. A, 1994, **566**: 483c
- 18 Clare R B, Strottman D. Phys. Rep., 1986, **141**: 177
- 19 Ornik U, Weiner R M, Wilk G. Nucl. Phys. A, 1994, **566**: 469c
- 20 Dias de Deus J, Milhano J G. Nucl. Phys. A, 2007, **795**: 98
- 21 LI B A, KO C M. Phys. Rev. C, 1995, **52**: 2037
- 22 ZHANG B. Comput. Phys. Commun., 1998, **109**: 193
- 23 Albacete J L. arXiv:0707.2545 [hep-ph]
- 24 WANG X N. Phys. Rev. D, 1991, **43**: 104
- 25 WANG X N, Gyulassy M. Phys. Rev. D, 1991, **44**: 3501
- 26 WANG X N, Gyulassy M. Phys. Rev. Lett., 1992, **68**: 1480
- 27 LIN Z W, KO C M, LI B A, ZHANG B, Pal S. Phys. Rev. C, 2005, **72**: 064901
- 28 Kharzeev D, Levin E, McLerran L. Phys. Lett. B, 2003, **561**: 93
- 29 Eskola K J, Kajantie K, Ruuskanen P V, Tuominen K. Nucl. Phys. B, 2000, **570**: 379
- 30 Sarkisyan E K G, Sakharov A S. arXiv:hep-ph/0410324, CERN-PH-TH/2004-213; Sarkisyan E K G, Sakharov A S. arXiv:hep-ph/0510191, AIP Conf. Proceedings, 2006, **828**: 35
- 31 Kokoulina E. Acta Phys. Pol. B, 2004, **35**: 295; Kokoulina E S, Nikitin V A. arXiv:hep-ph/0502224, Talk given at the XVII International Baldin Seminar "Relativistic Nuclear Physics and Quantum Chromodynamics", JINR, Dubna, Russia, Sept. 27 - Oct. 2, 2004; Ermolov P F, Kokoulina E S, Kuraev E A, Kutov A V, Nikitin V A, Pankov A A, Roufanov I A, Zhidkov N K. arXiv:hep-ph/0503254, Talk given at the XVII International Baldin Seminar "Relativistic Nuclear Physics and Quantum Chromodynamics", JINR, Dubna, Russia, Sept. 27 - Oct. 2, 2004
- 32 Kharzeev D, Kovchegov Y V, Tuchin K. Phys. Rev. D, 2003, **68**: 094013; Kharzeev D, Kovchegov Y V, Tuchin K. Phys. Lett. B, 2004, **599**: 23
- 33 Drescher H J, Hladik M, Ostapchenko S, Pierog T, Werner K. Phys. Rep., 2001, **350**: 93
- 34 Werner K, LIU F M, Pierog T. Phys. Rev. C, 2006, **74**: 044902; Werner K. Phys. Rev. Lett., 2007, **95**: 152301
- 35 LIU F H. Europhys. Lett., 2003, **63**: 193
- 36 LIU F H, Abd Allah N N, ZHANG D H, DUAN M Y. Int. J. Mod. Phys. E, 2003, **12**: 713
- 37 LIU F H, Abd Allah N N, Singh B K. Phys. Rev. C, 2004, **69**: 057601
- 38 LIU F H, LI J S, DUAN M Y. Phys. Rev. C, 2007, **75**: 054613
- 39 LIU F H, Panebratsev Y A. Phys. Rev. C, 1999, **59**: 1193
- 40 LIU F H. Phys. Rev. D, 2001, **63**: 032001
- 41 LIU F H. Phys. Rev. C, 2004, **69**: 067901
- 42 LIU F H. Phys. Rev. C, 2008, **78**: 014902
- 43 LIU F H. Nucl. Phys. A, 2008, **810**: 159
- 44 LIU F H, LI J S. Phys. Rev. C, 2008, **78**: 044602
- 45 Adcox K et al. (PHENIX collaboration). Phys. Rev. Lett., 2002, **89**: 212301